JOURNAL OF GEOPHYSICAL RESEARCH, VOL. 96, NO. A8, PAGES 14,051–14,064, AUGUST 1, 1991

Plasmoids as Magnetic Flux Ropes

MARK B. MOLDWIN AND W. JEFFREY HUGHES

Center for Space Physics and Department of Astronomy, Boston University, Boston, Massachusetts

Observational constraints on the magnetic topology and orientation of plasmoids is examined using a magnetic field model. We develop a magnetic flux rope model to examine whether principal axis analysis (PAA) of magnetometer signatures from a single satellite pass is sufficient to determine the magnetic topology of plasmoids and if plasmoid observations are best explained by the flux rope, closed loop, or large-amplitude wave picture. Satellite data are simulated by extracting the magnetic field along a path through our model of a magnetic flux rope. We then examine the results using PAA. We find that the principal axis directions (and therefore the interpretation of structure orientation) is highly dependent on several parameters including the satellite trajectory through the structure. Because of this we conclude that PAA of magnetometer data from a single satellite pass is insufficient to differentiate between magnetic closed loop and flux rope models. We also compare our model results to ISEE 3 magnetometer data of plasmoid events in various coordinate frames including principal axis and geocentric solar magnetospheric. We find that previously identified plasmoid events that have been explained as closed loop structures can also be modeled as flux ropes. We also searched the literature for previously reported flux rope and closed loop plasmoid events to examine if these structures had any similarities and/or differences. The results of our modeling efforts and examination of both flux rope and plasmoid events lead us to favor the flux rope model of plasmoid formation, as it is better able to unify the observations of various magnetic structures observed by ISEE 3.

INTRODUCTION

Observations by ISEE 3 of magnetic and plasma signatures in the deep magnetotail consistent with the passage of plasmoids lend support to the near-Earth-neutral-line/plasmoid model of substorms [e.g., *Hones*, 1976, 1977]. The plasmoid or near-Earth-neutral-line model of magnetic substorms has been very successful in explaining many of the phenomena observed in the Earth's magnetosphere during all phases of a substorm. The model predicts the buildup of magnetic flux in the tail lobes of the Earth's magnetosphere during periods of southward directed interplanetary magnetic field (IMF) due to magnetic merging on the dayside magnetopause. This growth phase [*Russell and McPherron*, 1973] is followed by the expansion phase of the magnetic substorm in which energy is deposited in the ionosphere and magnetosphere while flux is returned to the dayside. These models predict the formation of closed magnetic loops of plasma at substorm onset due to magnetic reconnection in the Earth's magnetotail. These closed loop structures have been named plasmoids and are subsequently ejected down the tail. The process of plasmoid formation and release consists of two stages. Initially, the closed loops formed within the plasma sheet by magnetic reconnection are surrounded by closed field lines that have not been reconnected. The plasmoid is ejected down the tail when the reconnection continues to lobe field lines that drape about the closed loops and pull the structure down the tail. Figure 1 shows this sequence of events. The first frame of the figure shows the tail near the end of the growth phase with magnetic flux building up in the tail. The second frame shows an X line forming where reconnection is taking place and the formation of the closed loop plasmoid. Reconnection continues into the lobe in the third frame, and these field lines wrap about the plasmoid and pull it down the tail, as seen in the last frame. This picture is two dimensional and only incorporates the noon-midnight meridional plane. In this two-dimensional picture the magnetic field within a plasmoid is closed on itself, a configuration we call a magnetic island. The plasma signatures of magnetic islands are tailward flow of a hot plasma and convecting isotropic energetic particle distributions [*Hones*, 1976; *Baker et al.*, 1984]. The only closed loop plasmoid magnetic signature originally identified was a bipolar trace in the geocentric solar magnetospheric (GSM) B_z coordinate [*Hones et al.*, 1984].

Hughes and Sibeck [1987] showed that the presence of a persistent and significant cross-tail magnetic field component, B_y, in the plasma sheet (as found by *Akasofu et al.* [1978] and *Lui* [1984]) alters the plasmoid formation process in such a way that helical field lines (flux ropes) are formed instead of closed loops. Therefore a three-dimensional picture is needed to examine the magnetic structure of plasmoids. These three-dimensional plasmoids are still connected to the Earth at their ends because of the finite extent of the reconnection region. If reconnection proceeds more rapidly at the center of the magnetotail, open field lines wrapped about the flux rope will bend or bow the structure antisunward. The plasmoid will be released when reconnection occurs at the ends of the structure. Flux rope signatures are expected to be similar to those of closed loop plasmoids and are a bipolar trace (in either the north-south or the east-west direction), a significant field maxima at the center of the event (due to the axial and/or azimuthal field component), and a double-peak signature in the direction perpendicular to the flux rope's bipolar signature for a spacecraft passage off axis to the structure [*Russell and Elphic*, 1979; *Sibeck et al.*, 1984; *Siscoe et al.*, 1984]. The plasma signatures are expected to be identical to closed loops [*Sibeck*, 1990].

Observations of structures with flux rope characteristics were also seen in the deep tail by ISEE 3 [*Sibeck et al.*, 1984; *Siscoe et al.*, 1984; *Scholer et al.*, 1985] and in the near-Earth tail by ISEE 1/2 [*Elphic et al.*, 1986]. Even though flux rope

Paper number 91JA01167.
0148-0227/91/91JA-01167$05.00

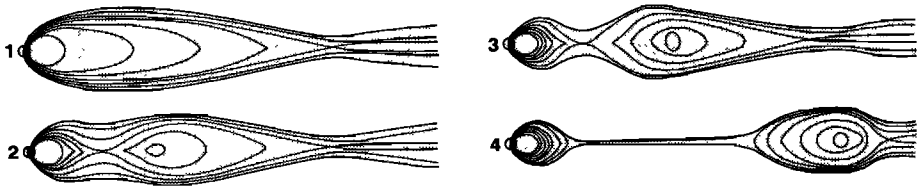

Fig. 1. The change in configuration of the magnetotail during a magnetospheric substorm. (Adapted from *Hones* [1977].)

and plasmoid structures have similar characteristics and have even been seen in succession of one another [*Siscoe et al.*, 1984], they have been separated into two different classes. *Sibeck et al.* [1984] pointed out three differences between the observed flux ropes and plasmoids. First, the magnetic field strength is as strong in the center of the flux ropes as in the lobes, whereas weaker fields are expected as the spacecraft samples the interior of a closed loop plasmoid [*Stern*, 1979]. Second, no double-peaked magnetic field signature has been reported in the direction perpendicular to the plasmoid's bipolar signature, as is seen in the three reported flux rope events. Finally, no bipolar B_y signature has been reported for plasmoids, while one of the three flux ropes has this characteristic.

Principal axis analysis (PAA) has been used in an attempt to determine the orientation of magnetic flux ropes in the tail [*Sibeck et al.*, 1984; *Elphic et al.*, 1986; *Slavin et al.*, 1989] and the Venus ionosphere [*Elphic et al.*, 1980; *Elphic and Russell*, 1983], and thus their axial field components. *Elphic and Russell* [1983] found, by assuming that the flux rope was cylindrically symmetric and that the spacecraft passed close to the axis of the flux rope, that the orientation of the flux rope could be determined by casting the magnetometer data into a principal axis coordinate frame. In the case of the Venus flux ropes, *Elphic et al.* [1980] and *Elphic and Russell* [1983] showed that the maximum variance direction corresponds to the axis of the flux rope, and the bipolar trace is found in the intermediate direction. The flux ropes observed in the near-tail by *Elphic et al.* [1986], however, had a weaker axial field; so the axis of the flux rope was along the intermediate variance direction. The deep magnetotail flux ropes observed by *Sibeck et al.* [1984] were assumed to have their axis oriented parallel to the maximum variance direction. The physical dimensions of a plasmoid, approximately 100 R_E in diameter and a few times 10 R_E in height [*Slavin et al.*, 1989], necessarily preclude the possibility for cylindrical symmetry. Also, the inability to uniquely determine the trajectory through the deep tail plasmoids prevents the identification of close impact passes. Nevertheless, several workers used PAA and the results of *Elphic and Russell*'s [1983] study of close impact passes of cylindrically symmetric flux ropes to determine the orientation of plasmoids [*Slavin et al.*, 1989; *Sibeck et al.*, 1984].

A third alternative picture of plasmoid observations has been proposed by *Lee et al.* [1988]. They propose that large-amplitude waves on the plasma sheet traveling down tail could give the expected bipolar signature of a plasmoid. In this picture the plasmoid is not a distinct structure but a perturbation or wave on the preexisting plasma sheet. Evidence for the north-south motion of the plasma sheet boundary layer with velocities of up to 100 km s^{-1} has been reported by *Richardson and Cowley* [1985].

These three pictures of plasmoid formation and evolution predict completely different topological structures. Closed loop plasmoids are completely isolated structures once their formation process begins, whereas flux ropes may remain connected to the Earth. In contrast, large-amplitude waves require no new magnetic field line topological structure. This topological difference might have ramifications on the dynamics and configuration of the Earth's magnetotail. Hence the determination of the three-dimensional structure of plasmoids is important to understanding the configuration of the dynamic magnetotail.

The goal of this paper is twofold: (1) to determine if principal axis analysis of magnetic field observations from a single spacecraft pass is sufficient to distinguish between flux ropes and isolated magnetic islands (i.e., can PAA be used to determine plasmoid orientation?) and (2) to determine if the ISEE 3 magnetometer observations of plasmoids are better explained by the flux rope, closed loop, or large-amplitude wave picture. To accomplish these goals, we develop a magnetic field model of a flux rope. We then simulate spacecraft observations by extracting the magnetic field along a path through the structure. The simulated data are then transformed into a principal axis coordinate frame, and the relationship between the structure's orientation and the PAA directions is determined. We find that the direction of the principal axis coordinates, determined from a satellite pass through a flux rope, is extremely dependent on a number of parameters, including the path of the satellite through the structure. Therefore the ability to determine a noncylindrical symmetric flux rope's orientation by PAA of a single satellite pass is questionable. Simulations are also compared with ISEE 3 magnetometer data in both GSM and PAA coordinates. We compare the locations of the plasmoid boundaries in our model with those identified in the ISEE 3 data. We also discuss previously published plasmoid and flux rope events to determine their respective characteristics and to determine if they have any similarities and/or differences. We find that the flux rope model of plasmoid formation is better able to unify the observations of various magnetic structures observed in the deep geotail and show that the ISEE 3 magnetometer observations that have been interpreted as plasmoids [*Hones et al.*, 1984; *Scholer et al.*, 1985; *Slavin et al.*, 1989] are also consistent with reported flux rope structures as well as with results from our flux rope model.

MODEL DESCRIPTION

We model the magnetic field topology of plasmoids with a $2\frac{1}{2}$-dimensional representation (i.e., B_y finite but $\partial/\partial y \equiv 0$) that can create the three-dimensional characteristics of magnetic flux rope plasmoids. Even though quantities in our

model vary only in two dimensions, three dimensions are required to describe the magnetic topology, hence our use of the term $2\frac{1}{2}$-dimensional. The magnetic structure created in this model consists of an elliptical field structure with a rigid boundary. We follow the approach of *Farrugia et al.* [1987] in determining the magnetic field outside our structure to mimic the magnetic lobe field. The axial field is constrained to satisfy MHD equilibrium. The currents required to generate these fields are also calculated. The three-dimensional structure created is representative of the lobes of the Earth's magnetotail draped about the flux rope. The plasma sheet is modeled as an infinitely thin current sheet.

This magnetic field model explicitly satisfies $\nabla \cdot \mathbf{B} = 0$. The elliptical plasmoid structure is described by these equations:

$$B_x = -B_{p0}\left(\frac{r^2}{L_0^2}\right) \exp\left(\frac{-r^2}{L_p^2}\right) \sin(\theta) \tag{1}$$

$$B_y = \frac{B_{f0}}{2}\left[\cos\left(\frac{\pi r}{L_f}\right) + 1\right] + B_{y0} \tag{2}$$

$$B_z = \frac{B_{p0}}{\zeta}\left(\frac{r^2}{L_0^2}\right) \exp\left(\frac{-r^2}{L_p^2}\right) \cos(\theta) \tag{3}$$

B_{p0}, L_0, and L_p are the characteristic field strength and scale lengths of the "plasmoid" field, respectively. θ and r denote the azimuthal and radial cylindrical coordinates referenced to the axis of the flux rope, which is in the y direction. They are

$$r = \sqrt{x^2 + (\zeta z)^2}$$
$$\theta = \arctan\left(\frac{\zeta z}{x}\right) \tag{4}$$

where ζ is the ratio of semimajor axis to semiminor axis length. The B_y magnetic component is constrained to satisfy MHD equilibrium or, more specifically, $(\mathbf{J} \times \mathbf{B})_y = 0$. This relationship requires the contours of the B_y field to be aligned with the magnetic field components in the x-z plane. B_{y0} is the value of the B_y field in the lobes, and $(B_{f0} + B_{y0})$ is the value of the B_y field at the center of the plasmoid. The parameter L_f is the length of the semimajor axis and determines the size of the flux rope. The B_y field is set to B_{y0} outside the structure. The field strength at the center of the plasmoid is entirely due to the axial field component. B_y is further constrained to have a maxima at the center of the structure and smoothly decay to B_{y0} at the boundary of the plasmoid. We arbitrarily chose the cosine function shown above that satisfies the requirements of $\nabla \cdot \mathbf{B} = (\mathbf{J} \times \mathbf{B})_y = 0$ as well as those stated above. In the limit of $B_y \to 0$, this flux rope becomes a closed loop with zero field strength at the center. At the other extreme, if $B_{y0} \geq B_z$ (at $r = a$ and $\theta = 0$ or π) and $\zeta \to 1$, the flux rope becomes more like the Venus flux ropes (i.e., cylindrical symmetric, strong axial field structures).

The lobe field is derived by examining an incompressible plasma flow past an elliptical cylindrical obstacle as was done by *Farrugia et al.* [1987] for the case of axially symmetric flux transfer events. The fields are given by these equations:

$$B_x = B_{s0}\left[1 - \frac{L_f^2}{r^2}\cos(2\theta)\right] \tag{5}$$

$$B_z = -B_{s0}\frac{L_f^2}{r^2}\sin(2\theta) \tag{6}$$

$(B_{s0}^2 + B_{y0}^2)^{1/2}$ is the lobe field strength at infinity. The projection of the field lines onto the x-z plane is plotted in Figure 2*a*. The parameters that define the structure are $B_{p0} = 40$ nT, $\zeta = 3$, $B_{s0} = 8$ nT, $L_p = L_0 = 3$, $B_{f0} = 4$ nT, $B_{y0} = 1$ nT, and $L_f = 5.6$. This particular structure will be used as the reference structure throughout this paper. The currents parallel to the flux rope axis are shown in a contour plot in Figure 2*b*. The current structure of the plasmoid is coaxial in nature with the main core current aligned with the axial magnetic field surrounded by the current sheet needed at the separatrix of the plasmoid and lobe/neutral sheet fields. The required currents at the boundary of the plasmoid structure to separate the strong lobe field from the weak field observed at the edge of the plasmoid is a previously undiscussed feature of plasmoids. This sharp boundary will be discussed later in the context of defining the plasmoid structure proper.

The contour plot of the total magnetic field is displayed in Figure 2*c*. The maximum lobe or exterior field strength is found at the "top" and "bottom" of the structure ($\theta = \pi/2$, $3\pi/2$) where the field is twice that in the lobe, B_{s0}. Physically, this is due to the bunching or compression of the lobe field due to the passage of the plasmoid. This is consistent with *Slavin et al.*'s [1984] traveling compression region (TCR) model where, because of the large vertical (north-south) extent of plasmoids, the lobe is compressed against the magnetopause boundary enhancing the B_x field strength in the lobes. The TCR signature would be observed if the spacecraft passed above or below a plasmoid without actually being engulfed by it. This increased magnetic pressure is also the physical cause of the elliptical shape of the plasmoid. There is a minimum in field strength at the leading and trailing edges ($\theta = 0$, π and $r = a$). This relaxing of magnetic pressure also contributes to the elliptical nature of the plasmoid. The maximum in magnetic field strength at the top and bottom of the plasmoid implies that a finite plasma pressure is required in the lobes for a structure in static equilibrium. However, in reality, dynamic pressure effects must play a role in balancing the total pressure in the two regions, but these effects are not included in our model. The implications of neglecting dynamic pressure effects will be discussed later.

After a magnetic structure is calculated, different experiments are run consisting of sampling the magnetic field along some path through the structure (a satellite pass). The magnetic field time series so generated is cast into a principal axis coordinate system by determining the direction of minimum variance. The maximum and intermediate variance directions complete the right-handed triad. This orders the data within the magnetic flux rope and, for special cases when the satellite passes close to the axis of the flux rope, reduces the field variations into two dimensions (see *Sonnerup and Cahill* [1967] for details), and simulates what has been routinely done with observations.

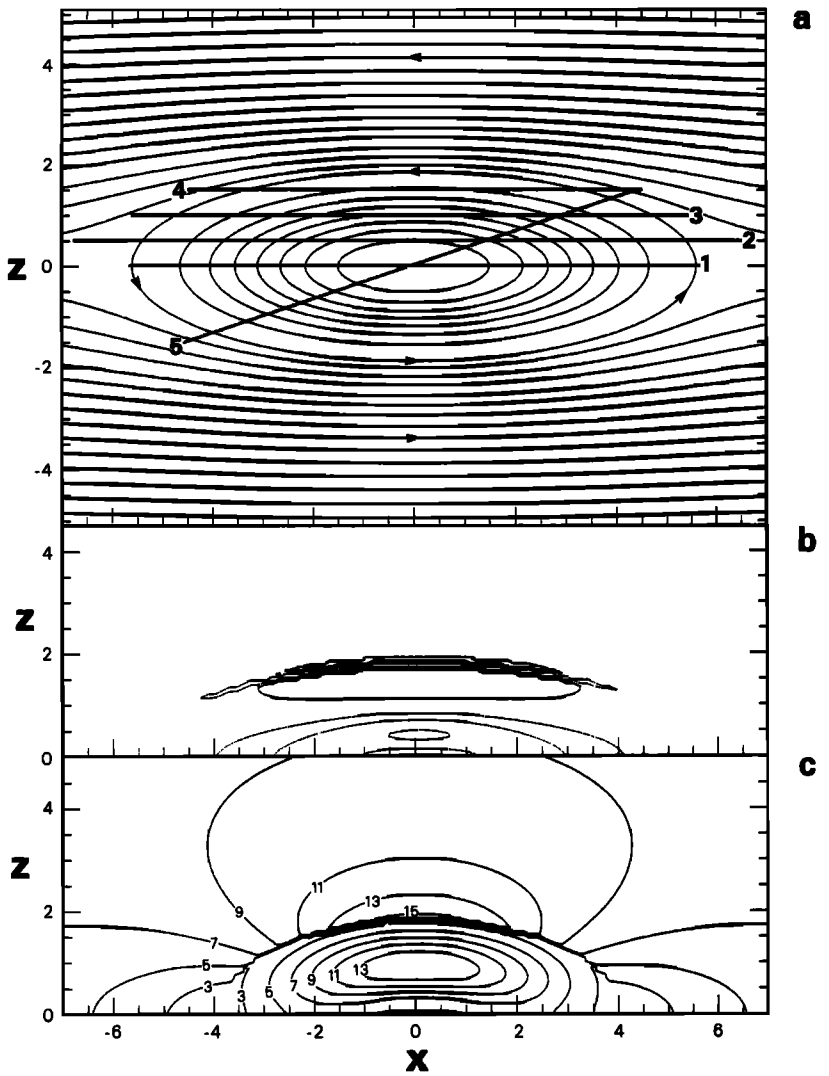

Fig. 2. (*a*) The magnetic topology of a plasmoid modeled by equations (1)–(6) depicted in the noon-midnight meridional plane. See text for the parameter values used. The numbered lines through the structure represent satellite trajectories. (*b*) A contour plot of the axial currents J_y required by the magnetic field configuration of the plasmoid depicted in Figure 2*a*. The solid line corresponds to positive J_y; dashed lines correspond to negative J_y. (*c*) A contour plot of the total magnetic field strength of the plasmoid in Figure 2*a*. Contour values are in nanoteslas. The asymptotic loop field strength is 8.1 nT.

FLUX ROPE ORIENTATION

We used the model to test the relationship between the orientation of a noncircular symmetric flux rope and the principal axis directions derived from a single satellite pass through the structure. *Elphic and Russell* [1983] showed that the orientation of a cylindrically symmetric flux rope can be determined if the satellite passed close to the center of the structure. In the case of the flux ropes observed in the Venus ionosphere (which have a strong axial field and a length along the symmetry axis much greater than their diameter), the maximum variance direction is parallel to the symmetry axis of the flux rope. The flux ropes observed in the near-Earth tail by ISEE 1 and 2 [*Elphic et al.*, 1986] have a weaker axial field than the Venus flux ropes; therefore the symmetry axis of the structure was assumed to lie parallel to the intermediate variance direction. However, deep magnetotail flux rope plasmoids are not cylindrically symmetric [*Hones et al.*, 1984; *Slavin et al.*, 1989], and their relative axial field strength can be highly variable; therefore the orientation of the flux rope is more difficult to determine.

Included in Figure 2*a* are five different satellite paths labeled 1–5. The corresponding magnetic time series for passes 1, 2, and 3 are shown in Figure 3 in GSM Cartesian coordinates and in Figure 4 in PAA coordinates, with the maximum variance (B_1), intermediate variance (B_2), and minimum variance (B_3) displayed top to bottom. The principal axis direction vectors for these three paths are shown in Table 1. Note the PAA signature for all three paths are very similar, but each path gives a principal axis direction reminiscent of a different structure. Path 1 gives the signatures and principal axis directions of a flux rope aligned perpendicular to the x axis. Path 3 gives a virtually identical signature but gives the principal axis directions consistent with a closed loop. Path 2 has its intermediate variance direction pointing ~45° between the x and y axis. Again, by just changing the impact parameter through the structure one

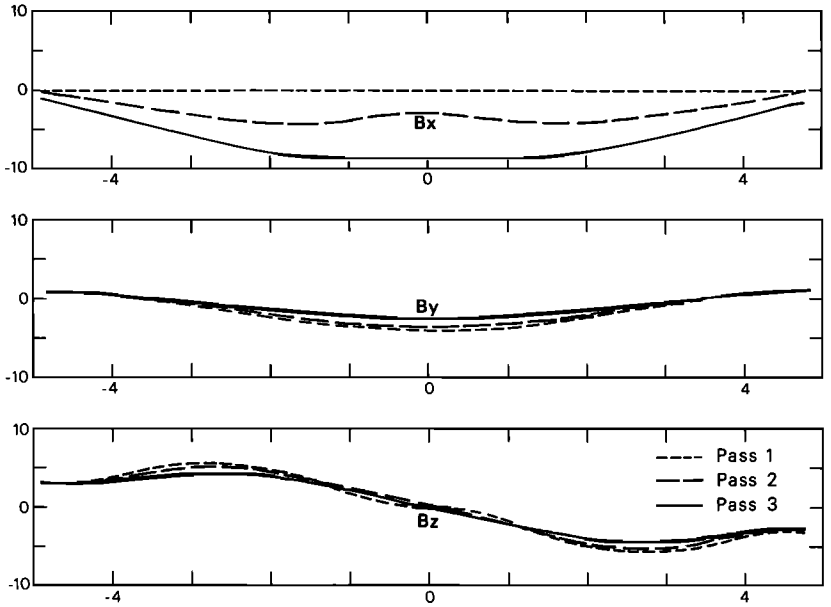

Fig. 3. The magnetic field in GSM coordinates observed by spacecraft moving along the trajectories numbered 1–3 shown in Figure 2*a*.

can create PAA signatures and directions consistent with both the flux rope and closed loop picture. Paths 1 and 3 meet the criteria for *Elphic and Russell*'s [1983] small impact parameter, namely, the ratio of the square of the variance in the maximum variance direction to the square of the variance in the minimum variance direction is greater than or equal to 100 ($\sigma_1^2/\sigma_3^2 \geq 100$). This criterion was used to determine how close to the center of the structure the spacecraft passed. Pass 2, which had a smaller impact parameter than path 3, nonetheless does not meet the above criteria. However, as Figure 4 shows, the PAA signatures of all three paths are very similar. Therefore PAA of noncylindrically symmetric structures from a single satellite pass is insufficient to determine the orientation and hence the topology of the structure.

Path 5 makes an angle of 20° to the current sheet. This would require a north-south motion of the neutral sheet of ~300 km s^{-1} for a plasmoid moving down the tail with a velocity of ~900 km s^{-1}. *Forbes et al.* [1981] found that the neutral sheet waves and flaps with an amplitude of ~100 km s^{-1} at near-Earth distances as measured by ISEE 1/2. *Richardson and Cowley* [1985], using ISEE 3 data, found the north-south motion of the neutral sheet boundary layer to be highly variable and ranged in velocity from ~20–300 km s^{-1} with an average of 99 ± 100 km s^{-1}. Combined with their average for the speed of the plasmoid of 890 ± 150 km s^{-1}, trajectories of ~20° to the neutral sheet are plausible. Path 4 was chosen to examine the effect of a satellite trajectory that passed near the edge of a plasmoid.

The parameters determined by casting the magnetic field variations along the five paths shown in Figure 2*a* into a principal axis coordinate frame are given in Table 1. Notice that the maximum and intermediate variance directions lie predominantly along a different axis for each pass through

TABLE 1. The Principal Axis Coordinates of Passes 1–5 Shown in Figure 2*a*, Including Average Magnetic Field Strength, Deviation, and Direction Vectors

Path	Axis	⟨B⟩	σ	Direction Vector
1	maximum variance	0.005	3.91	(0.000, −0.006, 0.999)
	intermediate variance	3.85	1.61	(0.00, 0.999, 0.006)
	minimum variance	−0.017	0.005	(1.00, 0.000, 0.00)
2	maximum variance	0.00	3.58	(0.00, −0.00, 0.999)
	intermediate variance	4.17	2.04	(−0.598, 0.801, 0.000)
	minimum variance	−0.301	0.599	(0.802, 0.598, 0.000)
3	maximum variance	1.06	3.13	(0.190, −0.08, 0.977)
	intermediate variance	5.03	3.09	(−0.888, 0.408, −0.210)
	minimum variance	−1.69	0.299	(0.417, 0.908, 0.00)
4	maximum variance	−7.05	2.57	(0.975, −0.217, −0.003)
	intermediate variance	0.016	2.42	(0.001, −0.009, 0.999)
	minimum variance	0.567	0.174	(0.217, 0.976, 0.008)
5	maximum variance	−0.254	6.46	(−0.670, 0.02, 0.742)
	intermediate variance	3.34	1.82	(0.02, 0.999, 0.009)
	minimum variance	−1.56	1.22	(0.742, −0.02, 0.670)

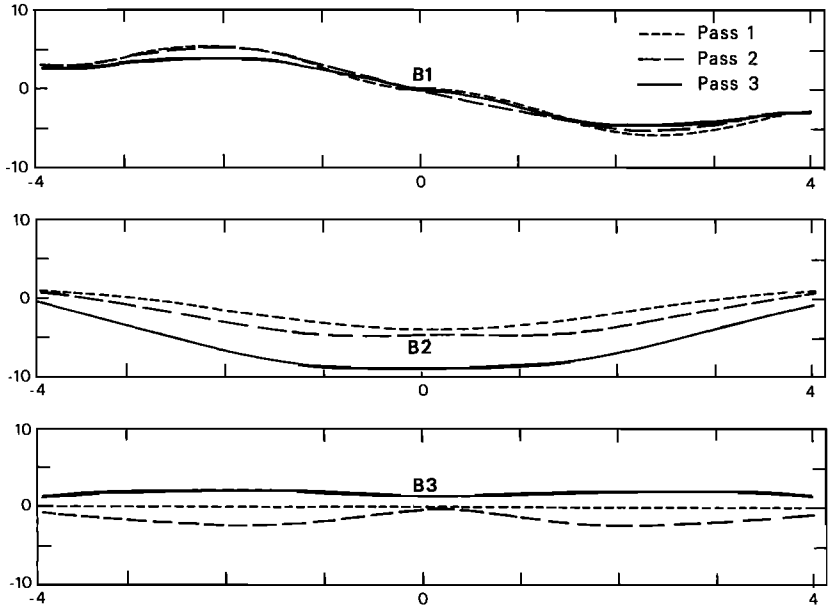

Fig. 4. The magnetic field shown in Figure 3 transformed in PAA coordinates.

the same structure. The minimum variance direction also changes from pass to pass. Figure 5 shows graphically how the PAA directions change with pass through the structure. The figure is a two-dimensional polar plot representing the three GSM directions. The circles are a projection onto the x-y plane of half the unit sphere. The symbols show where the principal axis direction vectors intersect the unit sphere. Thus the angle a vector makes with the x-y plane is plotted radially, while the angle the projection of the vectors onto the x-y plane makes to the x or y axis is plotted azimuthally. A vector aligned along the z axis would be located at the center of the plot, whereas a vector with no z component would be on the edge. The symbols represent the different components of the PAA direction. The square corresponds to the maximum variance direction, the circle corresponds to the intermediate variance direction, and the triangle corresponds to the minimum variance direction. As can be seen from Figure 5, the maximum variance direction varies considerably depending on the pass. The intermediate and minimum variance directions also change from pass to pass. This ambiguity makes it difficult to determine the orientation of a flux rope, making it difficult to differentiate between a closed magnetic loop and a flux rope on the basis of a single spacecraft trajectory. Again, this ambiguity adds to the difficulty of determining flux rope orientation by PAA.

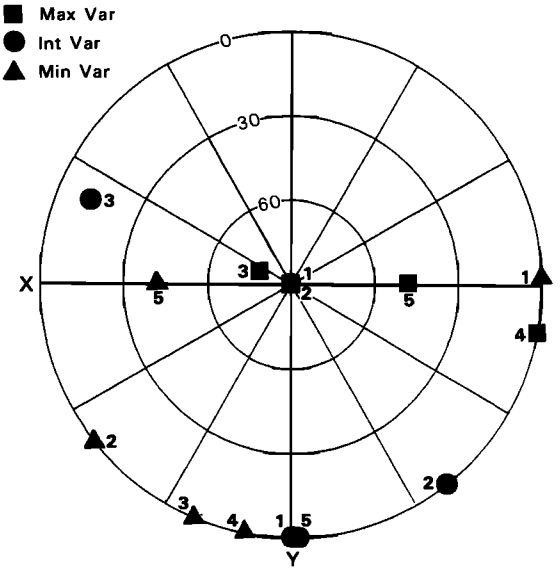

Fig. 5. A polar plot of the three principal axis direction vectors derived from the magnetic field variation along the five passes through the modeled structure. Each pass corresponds to a different trajectory through the structure. Notice how the directions of the PAA coordinate frames change from pass to pass. Note, at the center of the plot, corresponding to the principal axis vector parallel to $\hat{z}$, that there are three symbols overlapping (the maximum variance points for passes 1 and 2 and the intermediate variance point for pass 4, which is not labeled).

Another complication in determining the flux rope plasmoids orientation is that the relative strengths of the axial and azimuthal fields are difficult to measure and appear to be highly variable between events. By changing the relative strength of the axial to azimuthal field, one can get the same PAA signatures but with completely different principal axis directions. The effect of increasing the axial field (B_{f0}) or the "twist" of the flux rope has similar effects on the results of PAA as does changing the trajectory. Figure 6 shows the PAA directions for three identical passes through similar plasmoids that have different axial field strengths. The model structure used is the same as that shown in Figure 2, and pass 2 was the satellite path used in all three examples. The only parameter changed was B_{f0}, which is the strength of the y axial field at the center of the structure. The three different structures used had $B_{f0} = 0$ (closed loop), $B_{f0} = \frac{1}{2}B_{s0}$, and B_{s0}, where B_{s0} is the lobe field strength far from the structure. Figure 6 shows that as the twist or magnitude of B_{f0} decreases, the intermediate direction rotates from the y to x direction. This corresponds to the structure changing from a flux rope with a strong axial field to a closed loop.

Very similar behavior is observed by changing the ellip-

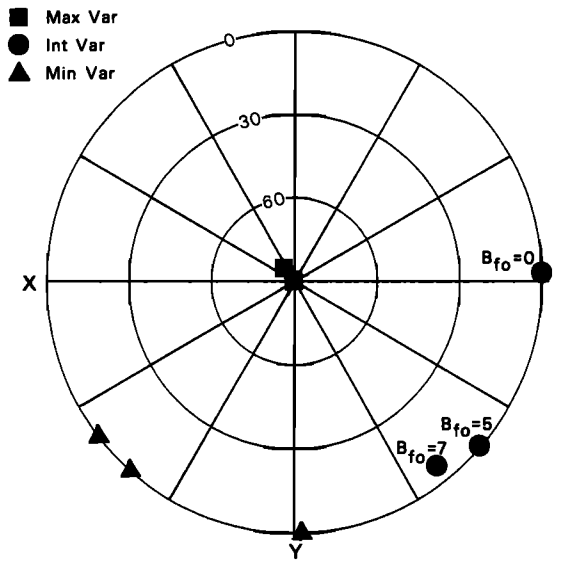

Fig. 6. A polar plot showing how the three principal axis direction vectors change with the "twist" of the flux rope. The three sets of vectors are derived from the magnetic variations along the same path through the structure, but in each case the value of B_{f0} is changed. Two maximum variance symbols lie on top of each other at the center of the diagram.

ticity of the plasmoid. The x extent of a plasmoid is typically from 40 R_E to 100 R_E, while the z dimension cannot be more than the tail diameter, which is typically tens of Earth radii. The ellipticity therefore can range from approximately circular to highly elongated. Figure 7 shows the progression of PAA directions obtained by changing the ellipticity of the structure and keeping the path and all other parameters the same. Again, the structure represented by Figure 2 and path 2 was used. The values of the ellipticity parameter used for the three structures were $\zeta = 1$, 2, and 2.5. As the plasmoid changes from circular to highly elliptical, the intermediate

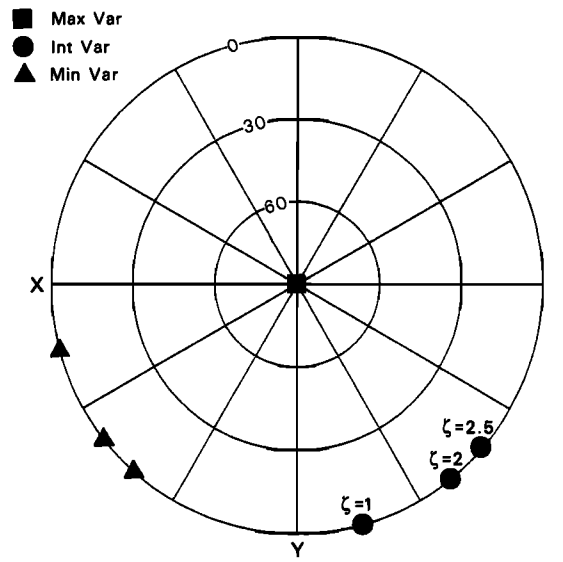

Fig. 7. Similar to Figure 6 but for three different values of ζ, the ratio of the semimajor to the semiminor axis of the elliptical plasmoid. The three symbols representing the maximum variance direction all lie at the center of the diagram.

variance direction moves from the y to the x direction. This is the same behavior as that observed by changing the structure from a flux rope to a closed loop. Therefore the determination of whether an observed plasmoid is a flux rope or a closed loop is further hindered by our inability to uniquely determine the shape of the plasmoid.

The effect of the satellite passing through a plasmoid oriented in an arbitrary direction with respect to the y or cross-tail direction was also investigated. As a closed loop plasmoid's symmetry axis is rotated from the cross-tail direction to being aligned along the Earth-Sun line, a spacecraft will initially sample magnetic field predominantly in the x-z plane and later fields in the y-z plane. Therefore a closed loop plasmoid could have the magnetic signature of a flux rope and vice versa. The effect of orientation of the structure on the directions of the principal axis is similar to the effect of "twist," ellipticity, and satellite trajectory and adds to the ambiguity of uniquely determining the topology of plasmoid events using PAA.

The basic reason for the failure of PAA in definitively determining the topology of a plasmoid lies in the necessary assumption that the satellite passes through the center of the structure. *Elphic and Russell* [1983] derived a criterion to determine how close to the center the satellite passed. They examined the ratio of the maximum and minimum variance and required it to be greater than 100. Plasmoid observations are very turbulent in comparison with the Venusian flux ropes examined by *Elphic and Russell* [1983] and often have $\sigma_1^2/\sigma_3^2 \sim 3$. Because of this, PAA cannot be used on a majority of the plasmoid events observed by ISEE 3.

Comparison to ISEE Observations

To determine if the ISEE 3 magnetometer observations are consistent with a flux rope picture, we compared the results of our model directly to observations. In order not to bias our modeled data, we simulated real observations by first generating a time series plot from a complete pass through a structure and used this plot to decide the point of entry and exit of the structure. A complete pass consists of a path that begins in the lobe, passes through the entire plasmoid, and ends in the lobe on the opposite side of entry. The key magnetic signature used in previous studies to determine the extent of the plasmoid is its bipolar trace in the GSM z direction or the north-then-south turning of the magnetic field vector. This is often difficult to do solely on the basis of the B_z bipolar signature owing to the often turbulent structure seen prior to and often incorporating the bipolar trace. The determination of the beginning and end of the plasmoid can have a profound effect on the PAA directions as well. We found that a better determination of entry into the actual plasmoid structure is the "core" signature. The core is defined as the maxima at the center of the structure. When the satellite enters the plasma sheet prior to entry into the plasmoid, the total $|B|$ magnitude drops from the lobe value to near zero and then recovers as it enters the plasmoid proper. We define the "beginning" and "end" of the plasmoid by the field minimums on either side of the "core" or field strength maximum that occur during the bipolar signature. Figure 8 is a composite of several plasmoid events and shows the GSM B_z and the total $|B|$. Notice that the extent of the core field comprises the majority of the total bipolar event. The lobe field in front of the plasmoid is

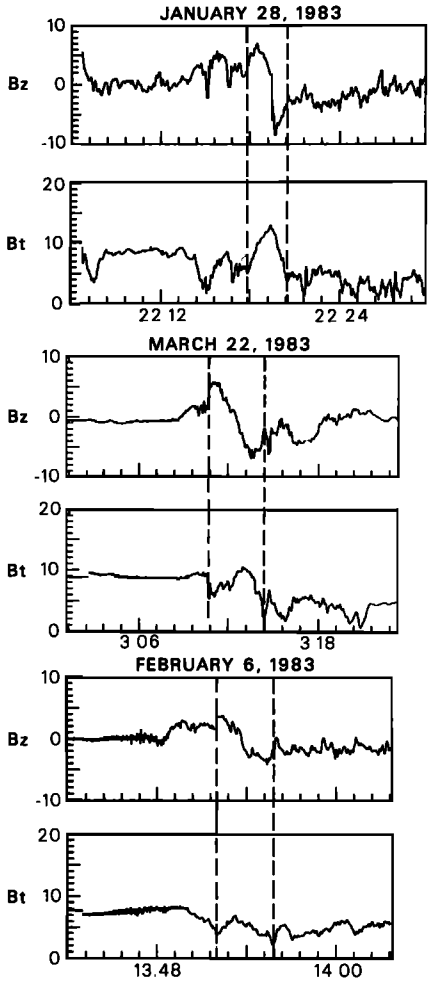

Fig. 8. Several plasmoid observations showing the B_z component and the total field magnitude. Note the bipolar trace in B_z and the field strength maximum (the "core" field) centered on the inflection point of the bipolar trace and extending for much of the bipolar trace. We determine the boundaries of plasmoids using the extent of the "core" field and the bipolar signature.

expected to exhibit the beginning of the bipolar trace due to the draping of the fields about the plasmoid proper. The "core" signature is therefore interpreted as the total plasmoid structure. The core field can be due to the B_x, B_y, or B_z component or a combination of any two of them. This portion of the pass was then transformed into a principal axis coordinate frame. These data were then directly compared with similarly extracted and transformed ISEE 3 data. We also compared the modeled results to ISEE 3 data in GSM coordinates.

The ISEE 3 magnetic field observations from March 22, 1983, which have been interpreted as a conventional plasmoid can also be modeled with the structure pictured in Figure 2. Pass 2 was used to reproduce the magnetometer observations. Figure 9*a* shows about 1 hour of ISEE 3 magnetometer data in GSM coordinates. At approximately 0310 UT the spacecraft leaves the north lobe and enters the neutral sheet. The large-amplitude magnetic oscillations seen are characteristic of the plasma sheet boundary layer [*Tsurutani et al.*, 1985]. The typical north-then-south turning of the B_z field component follows. A strong core field, predominantly in the B_x direction (9 nT), but with a significant B_y component (5 nT), is a signature of the plasmoid proper. Also in Figure 9*a* is the result of a pass through a modeled structure similar to that of Figure 2*a* that reasonably mimics the above plasmoid observation. The postplasmoid neutral sheet turbulence is not modeled. The magnetic observations for just the plasmoid (excluding the lobe and plasma sheet) are also modeled in PAA coordinates. Figure 9*b* shows the observational data (dotted lines) and the modeled data (solid lines). The ISEE 3 data were band passed filtered to remove all short-period oscillations (period of $\leq$60 s). The accuracy of fit is very good, lending support to the magnetic flux rope plasmoid picture. We did not search for the optimum fit to the data, as our purpose is simply to show that the data can be fit with a flux rope model. A number of different paths through the same model were found to give qualitatively comparable fits. The intermediate variance component is primarily due to the strong B_x field component of the flux rope. The maximum in its intensity occurs at the inflection point of the bipolar trace seen in the maximum variance direction.

Other plasmoid events can be successfully modeled by our flux rope model and have signatures that are characteristic of flux ropes. Figure 10 displays the ISEE 3 plasmoid event of January 28, 1983, at 2200 UT in GSM Cartesian coordinates. The plasmoid signatures of a bipolar trace in the B_z direction and a strong core field, in this case predominantly due to the field in the B_y direction, are clearly evident. This event is very similar to the flux ropes observed in the near-tail by ISEE 1/2 by *Elphic et al.* [1986]. The plasmoid event of February 6 at 0720 UT (which was identified by *Hones et al.* [1984] on the basis of the θ variation) can also be modeled as a flux rope and is shown in Figure 11.

Again, the optimum fit was not quantitatively determined, as these events can also be modeled with other flux rope models as well as closed loop models. However, modeling these events with a closed loop model would require unrealistic assumptions about the propagation direction and closed loop orientation. The problems with modeling plasmoids with the closed loop picture will be discussed in the next section.

Discussion

Comparison of Reported Flux Ropes to Plasmoid Events

Though flux rope and plasmoid signatures are very similar, *Sibeck et al.* [1984] listed three differences between the three flux ropes they reported and plasmoids. The first difference was that flux ropes have a significant core field that is comparable to the lobe field strength. Plasmoids were expected to have magnetic signatures of an O-type neutral line or closed loop, where the magnetic field strength decreases as the spacecraft approaches the center. Recently, *Slavin et al.* [1989] reported that plasmoid events have "enhanced internal magnetic fields which can exceed the magnitude of the adjacent lobe fields by as much as 10–20%." Whether this core field is due to an azimuthal or a strong axial field is the topic of current debate and differentiates closed loops from flux ropes. The flux rope picture requires the presence of an axial field, whereas the closed loop picture is two dimensional. All six plasmoids examined in this paper have significant core fields, while four of them have core fields that exceed the lobe field strength. The magnetic component

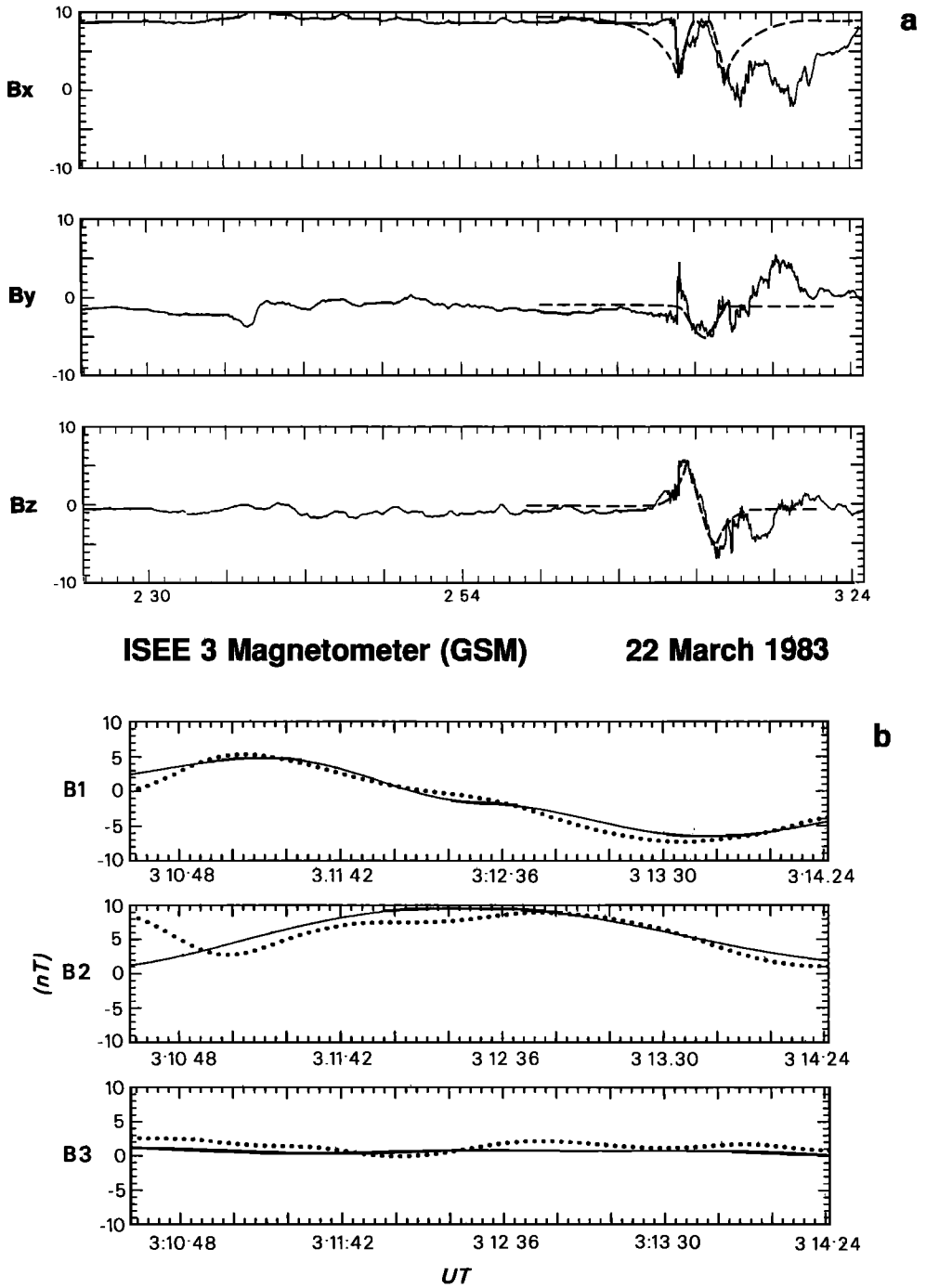

Fig. 9. (*a*) A comparison of the ISEE 3 magnetic field observations from March 22, 1983 (solid line), which have been interpreted as a conventional plasmoid, with a modeled fit (dashed line). ISEE 3 was at the GSM coordinates (−130.0, 11.1, 10.1). The model fit is obtained from pass 2 in Figure 2*a*. The traces are very similar, lending support to the magnetic flux rope plasmoid picture. (*b*) The model and observed magnetic variations within the plasmoid (i.e., excluding lobe and plasma sheet magnetic fields) in Figure 9*a* each transformed into its own principal axis coordinates. The ISEE 3 data were first low pass filtered and are shown with the dotted line.

that contributes to the core maximum is variable between the events with all of the events examined in this study having both B_x and B_y contributions to the core.

The second objection to flux ropes and plasmoids being the same structure was that the flux ropes observed had a double-peak signature perpendicular to the bipolar direction, whereas no plasmoid had been reported with this characteristic. Figure 12*a* is the ISEE 3 magnetometer data presented in GSM spherical coordinates for the plasmoid event of January 28, 1983. The distinct north-then-south turning of the θ magnetic component is clearly evident. A significant core field, exceeding the magnetic field strength in the lobes, is also present at the center of the structure, as determined by the inflection point of the bipolar signature. The magnetic trace in the ϕ direction has a double peak with the field approaching 270° twice, characteristic of an off-axis space-

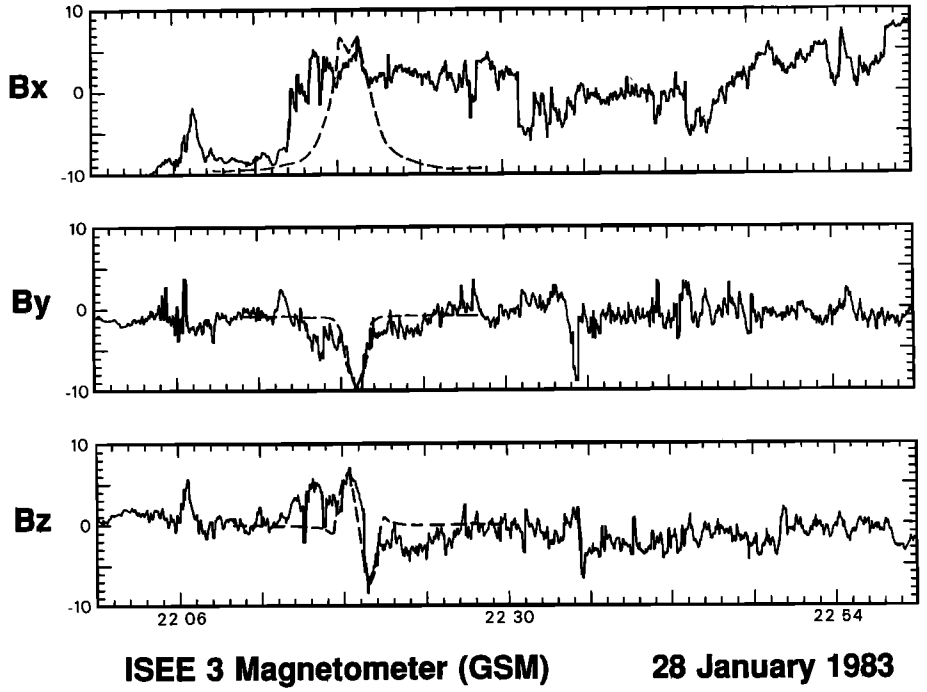

Fig. 10. The January 28, 1983, plasmoid event presented in GSM Cartesian coordinates together with a modeled fit. ISEE 3 was at the GSM coordinates (−216.3, 4.9, −6.4). Note that the core field is predominately due to the B_y field component. This is very similar to the flux rope observations made by *Elphic et al.* [1986] in the near-Earth magnetotail. The model fit is shown as a dashed line.

craft pass. This plasmoid event is strikingly similar to the three flux ropes presented by *Sibeck et al.* [1984], which are presented in Figures 12*b*, 12*c*, and 12*d*.

The third objection, that one of the three flux ropes seen had its bipolar trace in the B_y direction and not in the B_z direction as predicted by the two-dimensional plasmoid model, can be discounted by realizing that the early examination of the ISEE 3 data set for plasmoids expressly looked

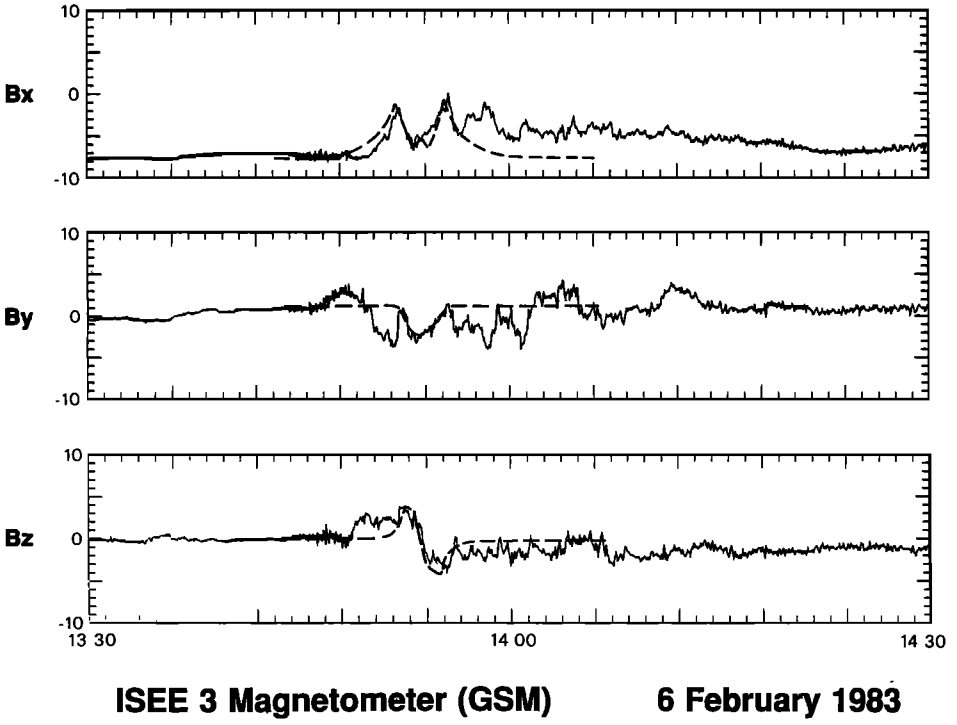

Fig. 11. The plasmoid event of February 6, 1983, presented in GSM Cartesian coordinates and its modeled fit. ISEE 3 was at the GSM coordinates (−220.4, 20.3, −9.0).

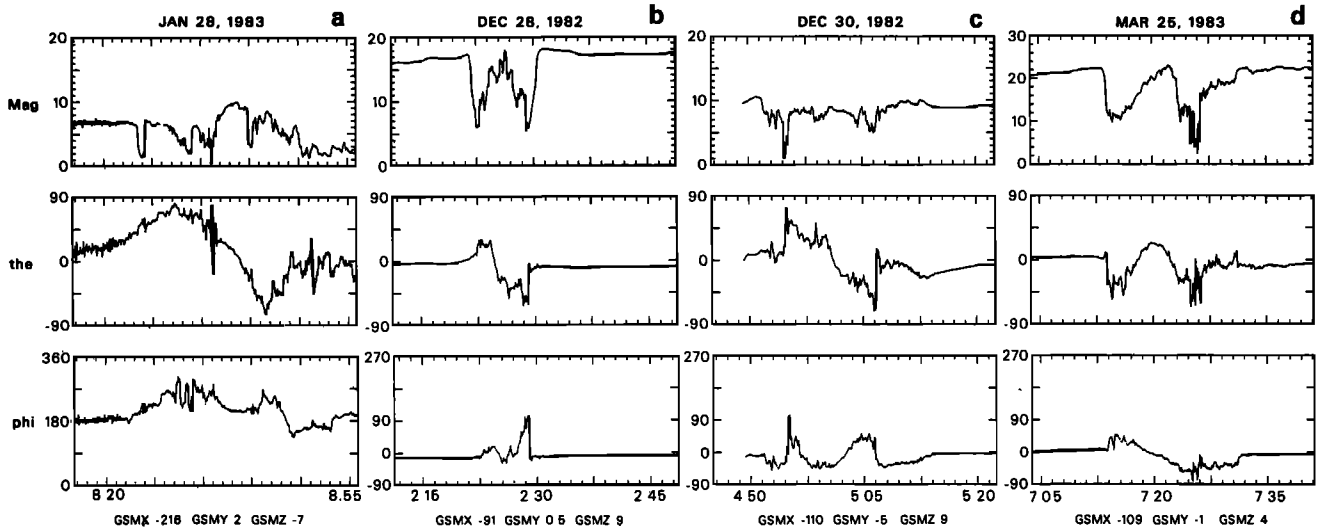

Fig. 12. (*a*) The January 28, 1983, plasmoid event depicted in GSM polar coordinates. The bipolar trace is evident in the θ direction. A double-peak signature is evident in the ϕ direction as the vector turns to 270° twice. (*b*, *c*, *d*) The three flux ropes identified by *Sibeck et al.* [1984]. Note the similarity between the three flux ropes and the January 28 plasmoid.

for the bipolar trace in the B_z direction [*Slavin et al.*, 1989; *Hones et al.*, 1984]. This is because the original plasmoid hypothesis was formulated only in the noon-midnight meridional plane and so did not even consider the third (y) direction. Figure 13 shows the ISEE 3 plasmoid event of January 26, 1983, in GSM Cartesian coordinates. In this coordinate frame it is evident that the bipolar signature is much more pronounced in the B_y direction than in the B_z direction. The event has been modeled as a flux rope, but the results are not presented. A reexamination of the ISEE 3 magnetometer data set for east-west bipolar signatures could discover many more flux rope plasmoids overlooked in the initial studies. The March 25 event identified by *Sibeck et al.* [1984] as a flux rope with its bipolar trace in the y direction was later interpreted as the signature of one and a half plasmoids by *Richardson et al.* [1989]. They argued that the event was actually two plasmoids with the south-north-south B_z field signature corresponding to the trailing half of one plasmoid followed by a second plasmoid. *Scholer et al.* [1985] and *Kennel et al.* [1986] supported *Sibeck et al.*'s [1984] original interpretation of the event as a single flux rope. Our modeling efforts confirm that this event is consis-

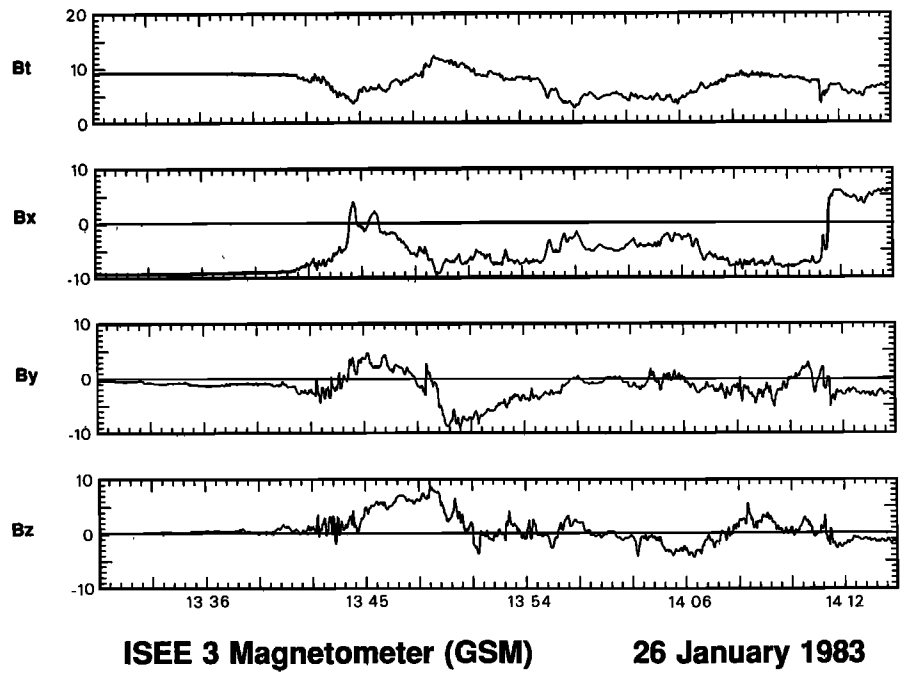

Fig. 13. The January 26, 1983, plasmoid event displayed in GSM Cartesian coordinates. ISEE 3 was located at the GSM coordinates (−213.5, −1.0, −6.5). The bipolar trace is evident in the B_y direction, while the core field is seen as a broad maximum in the B_z direction.

tent with that interpretation. If the event is actually two plasmoids and the spacecraft is not engulfed by the neutral sheet/plasmoid structures until it has passed half of the first plasmoid, we believe the TCR signature of the first plasmoid should at least be seen prior to the observed event. Therefore we believe the March 25, 1983, CDAW 8 event is a flux rope plasmoid with its symmetry axis apparently bent in the x-y plane.

Farrugia et al. [1987] showed that an external pass of a flux transfer event was capable of giving a flux rope signature due to the draping external field. This result is obviously reproduced with our model, since we use the *Farrugia et al.* [1987] formalism to represent our external field (the lobe). We considered whether TCRs could give flux rope signatures as well. TCRs have much weaker field signatures than the plasmoid events examined and are easily distinguished owing to their lack of an isolated core field in contrast to all six plasmoids examined in this study, which had very distinct core signatures. That signature is a depression of the field to values near zero before the field recovers to a strong single peak. TCRs exhibit the field enhancement, but not the field depressions. Thus TCRs cannot mimic the flux rope signature.

An Explanation for Plasmoid High $|B|$ Regions

The high $|B|$ core regions found in plasmoids by *Slavin et al.* [1989] were a new and unexpected result. The field in the core of a idealized closed loop structure surrounding an O-type neutral line should be weaker as a satellite approaches the center [*Stern*, 1979]. The flux rope picture provides a natural explanation for the high $|B|$ strengths observed in the center of many plasmoids. The axial core field, which differentiates flux ropes from closed loops, is the field component responsible for the significant core field seen in plasmoid events such as the January 28, 1983, event at 2200 UT. However, several of the plasmoid events examined contained significant and comparable field components in the GSM x and y direction. This can be interpreted in various ways. One possibility is that the plasmoid is aligned skewed in the x-y plane. Another is that the flux rope plasmoid is aligned parallel to the y axis (the same orientation as depicted in the two-dimensional closed loop plasmoid scenario) but has comparable axial and azimuthal field components and the satellite passes off axis through the structure. Principal axis analysis is unable to differentiate between these two pictures.

The determination of the origin of the strong core fields observed is obscured by the uncertainties in the trajectories of the satellite through the structure. As was shown in Figure 2 and the discussion that pertained to it, the principal axis component that corresponds to the core field is strongly dependent on how close the spacecraft passes to the center of the structure. The variety of directions that the core fields are found among the six plasmoid events examined in this paper can be satisfactorily explained by our flux rope model and appear to be due to each having different impact parameters to the axis of the flux rope. *Slavin et al.* [1989] explain the high core field by a mechanism similar to Slavin's TCR model. That is, the magnetic pressure of the lobes pushes the top and bottom of the plasmoid toward the center and hence enhances the B_x component near the edge of the plasmoid. Therefore a spacecraft that passes close to the plasmoid edge will sample a strong core field. *Fairfield et al.* [1989], however, found no evidence for a decrease in plasma pressure as one might expect if plasma is being squeezed out of the region. As will be discussed later, several plasmoid events have their core predominantly in the y direction and not the x direction, as the Slavin model would require. Additionally, if the spacecraft passed through the center of the plasmoid, it should sample near-zero field in the closed loop picture, whereas none of the plasmoids examined in this study and only one previously published possible plasmoid (see the third bipolar event in CDAW 8 interval F [*Richardson et al.*, 1989]) have a field minimum at the center of the pass.

Limitations of the Closed Loop and Large-Amplitude Wave Pictures

The expected signatures of flux ropes and closed loop structures are very similar because the closed loop forms one limit of flux ropes: the limit in which the cross-tail magnetic field is zero [*Sibeck*, 1990]. Though several plasmoid events are consistent with both the closed loop picture and a tight spiraled flux rope picture [*Slavin et al.*, 1989], several others are hard to reconcile with the closed loop picture. The January 26, 1983, event (shown in Figure 13) that has its bipolar trace in the y direction would require the symmetry axis of the closed loop to be aligned along the z axis. This can be done in the *Hughes and Sibeck* [1987] scenario owing to the connection of the flux rope to the two poles of the Earth in the initial stages of plasmoid formation. Results from three-dimensional MHD simulations of plasmoid formation with a finite B_y applied across the magnetotail show that the flux rope plasmoid formed does indeed twist about to align along the z axis (R. J. Walker, private communication, 1989). *Sibeck et al.* [1985] showed that the entire distant magnetotail can twist in the presence of a strong IMF B_y, and therefore the orientation of a magnetic structure embedded in the plasma sheet could also be expected to twist. The 2200 UT January 28, 1983, plasmoid event (shown in Figure 10) is also difficult to reconcile with the closed loop picture. The distinct maxima in the B_y component would require the symmetry axis of the plasmoid to be aligned along the magnetotail axis, with the spacecraft moving across the structure in the cross-tail direction. The traditional closed loop model has the symmetry axis in the cross-tail direction and the structure propagating downtail. This event is consistent with a strong axial field flux rope with its symmetry axis aligned in the cross-tail direction and propagating downtail. Flux rope plasmoids also can be aligned in various configurations in the magnetotail owing to the differential reconnection rates across the tail and their connection to the Earth at their formation.

As plasmoids move down the tail, they grow from their small sizes to large-scale structures with dimensions of the order of the size of the magnetotail [*Sibeck*, 1990]. Flux ropes have an axial field component to hold the structure together against the nonuniform forces and stresses along its length. Closed loop plasmoids do not have this field component to give it structural integrity and identity. The mechanism to hold a closed loop plasmoid together as it travels down the tail has not been addressed in the literature. Flux ropes also should eventually break apart even if flux ropes are not subject to any instabilities (such as current-driven

pinch instabilities). As the structure expands, its field strength should diminish; eventually the axial component will become too weak to tie the structure together, and the flux rope should be destroyed. A closed loop plasmoid should suffer this fate much earlier. As a flux rope grows in size, the axial field diminishes as r^{-2} (to conserve magnetic flux through the rope), whereas the azimuthal field decreases as r^{-1}, more slowly than the axial field.

Another feature of plasmoid observations that is not easily reconciled with the closed loop plasmoid picture is the possible heat flux observed inside plasmoids by *Fairfield et al.* [1989]. A heat flux is inconsistent with the classical closed loop plasmoid picture, whereas a heat flux could be compatible with a flux rope.

An alternative picture proposed to explain plasmoid observations has been presented by *Lee et al.* [1988]. They argue that a large-amplitude wave or tail oscillation mode traveling down tail could give the same bipolar signature expected for a plasmoid. Two difficulties with this picture have been raised by *Slavin et al.* [1989]: they are the inability of the large-amplitude wave or normal mode picture to explain the strong core field observed in plasmoids and the characteristic asymmetry and turbulence seen in the post-plasmoid plasma sheet. A third objection to the large-amplitude wave picture is that at the edge of the plasmoids examined in this study, the field is virtually aligned with GSM z with very little or no B_x component, suggesting the wave must have a very large amplitude sufficient to tilt the plasma sheet into the y-z plane.

Other Flux Rope Plasmoid Observations?

Other long-wavelength θ variation structures have been seen by ISEE 3 and include, besides the typical plasmoid north-south events, structures where the field rotates to large northward angles then to zero, south-north, and southward-then-zero orientations [*Tsurutani et al.*, 1987]. The flux rope model can explain both tailward (north-south signature) and earthward (south-north signature) moving plasmoids [*Hughes and Sibeck*, 1987], as well as the stagnant plasmoids seen by *Nishida et al.* [1986]. It can also explain the north-then-zero and south-then-zero events. Because reconnection does not proceed uniformly across the tail, the center of the flux rope plasmoid can be pulled down the tail faster than the flanks, bowing the rope. A spacecraft passing through this structure along a path near the flanks of the structure would first see a northward (southward) field variation, and then the θ component of the field would go to zero, since the spacecraft would begin to traverse down the axis of the structure. This is because the structure is uniform along its axis.

Limitations of Our Model

Our model is able to simulate the magnetic plasmoid observations of ISEE 3 in both principal axis coordinates and geophysical coordinates. It also offered a new way for determining the boundaries of the actual plasmoid structure (i.e., a way to differentiate the plasmoid from the surrounding neutral sheet). The flux rope model is also more general and flexible than the two-dimensional closed loop picture and therefore explains a wider range of plasmoid features. However, our model is limited in two basic respects. First, our model does not contain a neutral sheet explicitly. Since plasmoid formation is initiated in the plasma sheet and plasma sheet plasma is contained in and surrounds the plasmoid, our model is unable to simulate an entire spacecraft pass from lobe through plasma sheet into plasmoid and back out to the lobe again. However, this inability actually helps us determine the actual plasmoid signature by separating out the often complex plasma sheet signatures. Our flux rope model was developed to meet basic static MHD equilibrium and describes a static structure embedded in the magnetic lobes. Plasmoids with velocities of up to 1000 km s^{-1} are far from static and are affected by the magnetic tension forces and plasma pressure gradients pulling/pushing the plasmoid down the tail. Plasmoids are also constricted in the vertical direction by the magnetic pressure in the lobe and by the ram pressure due to their motion relative to the downstream plasma sheet. Examination of plasma data interior of the plasmoid also shows that there is a lack of pressure equilibrium inside the structure [*Fairfield et al.*, 1989].

SUMMARY AND CONCLUSIONS

The existence of a persistent and significant magnetic field component in the cross-tail direction (B_y) in the Earth's magnetotail drastically changes the magnetic topological picture of plasmoids. The change in the plasmoid's configuration with a B_y component present was described qualitatively by *Hughes and Sibeck* [1987] and has been modeled by *Birn et al.* [1989]. They found instead of isolated closed magnetic loops, flux ropes are formed. The flux rope model developed in this paper reproduces the plasmoid magnetic signatures seen by ISEE 3 showing that the observations are consistent with the flux rope picture. Flux rope plasmoids can have a bipolar trace in either the north-south or east-west direction, can have a significant axial core field that can exceed the magnetic field strength in the lobe, and can have many different orientations in the Earth's magnetotail. The flux rope picture unifies many of the magnetic structures seen in the magnetotail by explaining many of the observations with a single picture. The flux rope picture also eliminates many ambiguities and problems with interpreting the ISEE 3 plasmoid data with the closed loop or the wave/normal mode picture including the possible heat flux observed by *Fairfield et al.* [1989] which is incompatible with a closed loop structure but is quite consistent with a flux rope.

Principal axis analysis is, in general, a poor way of determining the symmetry axis and orientation of plasmoids observed in the tail. The directions of the principal axes are strongly dependent on the spacecraft trajectory through the structure as well as on the configuration, ellipticity, and "twist" of the structure. Therefore care must be taken in interpreting the orientation of plasmoids by principal axis analysis.

Our static $2\frac{1}{2}$-dimensional magnetic field model, though limited, suggested a concrete method of determining plasmoid boundaries based on the field strength maximum seen in the center of plasmoids and has been able to model many observations of plasmoids. The ramifications of flux rope plasmoids in terms of tail dynamics, auroral morphology, and plasmoid stability are questions that still need to be addressed. An important implication of our flux rope model

is that it shows the importance and relevance of thinking of the magnetosphere in three dimensions and demonstrates the importance of coordinated multiple-spacecraft magnetospheric missions such as Cluster.

Acknowledgments. The authors would like to thank J. A. Slavin for kindly providing us with the ISEE 3 magnetometer data (E. J. Smith, principal investigator) and for his helpful comments and encouragement. We also thank the two referees for their constructive suggestions and comments. This work was supported by the National Aeronautics and Space Administration under grant NAGW-1627.

The Editor thanks C. T. Russell and D. Sibeck for their assistance in evaluating this paper.

REFERENCES

Akasofu, S.-I., A. T. Y. Lui, C.-I. Meng, and M. Haurwitz, Need for a three-dimensional analysis of magnetic fields in the magnetotail during substorms, *Geophys. Res. Lett.*, *5*, 283, 1978.

Baker, D. N., S. J. Bame, R. D. Belian, W. C. Feldman, J. T. Gosling, P. R. Higbe, E. W. Hones, Jr., D. J. McComas, and R. D. Zwickl, Correlated dynamical changes in the near-Earth and distant magnetotail regions: ISEE 3, *J. Geophys. Res.*, *89*, 3855, 1984.

Birn, J., M. Hesse, and K. Schindler, Filamentary structure of a three-dimensional plasmoid, *J. Geophys. Res.*, *94*, 241, 1989.

Elphic, R. C., and C. T. Russell, Magnetic flux ropes in the Venus ionosphere: Observations and models, *J. Geophys. Res.*, *88*, 58, 1983.

Elphic, R. C., C. T. Russell, J. A. Slavin, and L. H. Brace, Observations of the dayside ionopause and ionosphere of Venus, *J. Geophys. Res.*, *85*, 7679, 1980.

Elphic, R. C., C. A. Cattell, K. Takahashi, S. J. Bame, and C. T. Russell, ISEE-1 and 2 observations of magnetic flux ropes in the magnetotail: FTEs in the plasma sheet?, *Geophys. Res. Lett.*, *13*, 648, 1986.

Fairfield, D. H., D. N. Baker, J. D. Craven, R. C. Elphic, J. F. Fennell, L. A. Frank, I. G. Richardson, H. J. Singer, J. A. Slavin, B. T. Tsurutani, and R. D. Zwickl, Substorms, plasmoids, flux ropes, and magnetotail flux loss on March 25, 1983: CDAW 8, *J. Geophys. Res.*, *94*, 15,135, 1989.

Farrugia, C. J., R. C. Elphic, D. J. Southwood, and S. W. H. Cowley, Field and flow perturbations outside the reconnected field line region in flux transfer events: Theory, *Planet. Space Sci.*, *35*, 227, 1987.

Forbes, T. G., E. W. Hones, Jr., S. J. Bame, and J. R. Asbridge, Substorm-related plasma sheet motions as determined from differential timing of plasma changes at the ISEE satellites, *J. Geophys. Res.*, *86*, 3459, 1981.

Hones, E. W., Jr., The magnetotail: Its generation and dissipation, in *Physics of Solar Planetary Environments*, edited by D. J. Williams, pp. 559–571, AGU, Washington, D. C., 1976.

Hones, E. W., Jr., Substorm processes in the magnetotail: Comments on 'On hot tenuous plasma, fireballs, and boundary layers in the Earth's magnetotail' by L. A. Frank, K. L. Ackerson, and R. P. Lepping, *J. Geophys. Res.*, *82*, 5633, 1977.

Hones, E. W., Jr., D. N. Baker, S. J. Bame, W. C. Feldman, J. T. Gosling, D. J. McComas, R. D. Zwickl, J. A. Slavin, E. J. Smith, and B. T. Tsurutani, Structure of the magnetotail at 220 R_E and its response to geomagnetic activity, *Geophys. Res. Lett.*, *11*, 5, 1984.

Hughes, W. J., and D. G. Sibeck, On the 3-dimensional structure of plasmoids, *Geophys. Res. Lett.*, *14*, 636, 1987.

Kennel, C., F. V. Coroniti, and F. L. Scarf, Plasma waves in magnetotail flux ropes, *J. Geophys. Res.*, *91*, 1424, 1986.

Lee, L. C., S. Wang, C. Q. Wei, and B. T. Tsurutani, Streaming sausage, kink, and tearing instabilities in a current sheet with applications to the Earth's magnetotail, *J. Geophys. Res.*, *93*, 7354, 1988.

Lui, A. T. Y., Characteristics of the cross-tail current in the Earth's magnetotail, in *Magnetospheric Currents Geophys. Monogr. Ser.*, vol. 28, edited by T. A. Potemra, pp. 158–170, AGU, Washington, D. C., 1984.

Nishida, A., M. Scholer, T. Terasawa, S. J. Bame, G. Gloeckler, E. J. Smith, and R. D. Zwickl, Quasi-stagnant plasmoid in the middle tail: A new preexpansion phase phenomenon, *J. Geophys. Res.*, *91*, 4245, 1986.

Richardson, I. G., and S. W. H. Cowley, Plasmoid-associated energetic ion bursts in the deep geomagnetic tail: Properties of the boundary layer, *J. Geophys. Res.*, *90*, 12,133, 1985.

Richardson, I. G., C. J. Owen, S. W. H. Cowley, A. B. Galvin, T. R. Sanderson, M. Scholer, J. A. Slavin, and R. D. Zwickl, ISEE 3 observations during the CDAW 8 intervals: Case studies of the distant geomagnetic tail covering a wide range of geomagnetic activity, *J. Geophys. Res.*, *94*, 15,189, 1989.

Russell, C. T., and R. C. Elphic, Observations of magnetic flux ropes in the Venus ionosphere, *Nature*, *279*, 616, 1979.

Russell, C. T., and R. L. McPherron, The magnetotail and substorms, *Space Sci. Rev.*, *15*, 205, 1973.

Scholer, M., B. Klecker, D. Hovestadt, G. Gloeckler, F. M. Ipavich, and A. B. Galvin, Energetic particle characteristics of magnetotail flux ropes, *Geophys. Res. Lett.*, *12*, 191, 1985.

Sibeck, D. G., Evidence for flux ropes in the Earth's magnetotail, in *Physics of Magnetic Flux Ropes, Geophys. Monogr. Ser.*, vol. 58, edited by C. T. Russell et al., pp. 637–646, AGU, Washington, D. C., 1990.

Sibeck, D. G., G. L. Siscoe, J. A. Slavin, E. J. Smith, S. J. Bame, and F. L. Scarf, Magnetotail flux ropes, *Geophys. Res. Lett.*, *11*, 1090, 1984.

Sibeck, D. G., G. L. Siscoe, J. A. Slavin, E. J. Smith, B. T. Tsurutani, and R. P. Lepping, The distant magnetotail's response to a strong interplanetary magnetic field B_y: Twisting, flattening, and field line bending, *J. Geophys. Res.*, *90*, 4011, 1985.

Siscoe, G. L., D. G. Sibeck, J. A. Slavin, E. J. Smith, B. T. Tsurutani, and D. E. Jones, ISEE 3 magnetic field observations in the magnetotail: Implications for reconnection, in *Magnetic Reconnection in Space and Laboratory Plasmas, Geophys. Monogr. Ser.*, vol. 30, edited by E. W. Hones, Jr., p. 240, AGU, Washington, D. C., 1984.

Slavin, J. A., E. J. Smith, B. T. Tsurutani, D. G. Sibeck, H. J. Singer, D. N. Baker, J. T. Gosling, E. W. Hones, Jr., and F. L. Scarf, Substorm associated traveling compression regions in the distant tail: ISEE 3 geotail observations, *Geophys. Res. Lett.*, *11*, 657, 1984.

Slavin, J. A., D. N. Baker, J. D. Craven, R. C. Elphic, D. H. Fairfield, L. A. Frank, A. B. Galvin, W. J. Hughes, R. H. Manka, D. G. Mitchell, I. G. Richardson, T. R. Sanderson, D. J. Sibeck, H. J. Singer, E. J. Smith, and R. D. Zwickl, CDAW 8 observations of plasmoid signatures in the geomagnetic tail: An assessment, *J. Geophys. Res.*, *94*, 15,153, 1989.

Sonnerup, B. U. O., and L. J. Cahill, Magnetopause structure and attitude from Explorer 12 observations, *J. Geophys. Res.*, *72*, 171, 1967.

Stern, D. P., The role of O-type neutral lines in magnetic merging during substorms and solar flares, *J. Geophys. Res.*, *84*, 63, 1979.

Tsurutani, B. T., I. G. Richardson, R. M. Thorne, W. Butler, E. J. Smith, S. W. H. Cowley, S. P. Gary, S.-I. Akasofu, and R. D. Zwickl, Observation of the right-hand resonant ion beam instability in the distant plasma sheet boundary layer, *J. Geophys. Res.*, *90*, 12,159, 1985.

Tsurutani, B. T., M. E. Burton, E. J. Smith, and D. E. Jones, Statistical properties of magnetic field fluctuations in the distant plasmasheet, *Planet. Space Sci.*, *35*, 229, 1987.

W. J. Hughes and M. B. Moldwin, Center for Space Physics and Department of Astronomy, Boston University, Boston, MA 02215.

(Received December 26, 1990;
revised April 4, 1991;
accepted April 22, 1991.)